Overburden pore pressure changes and their influence on 4D seismic

Rune M Holt*, NTNU; Andreas Bauer, SINTEF and NTNU; and Audun Bakk, SINTEF

Summary

Changes in seismic two-way travel time in the overburden can be attributed to pore pressure changes in the underlying reservoir. Since cap rock permeability is very small, these stress changes occur without drainage on short term, which means that, depending on stress path, pore pressure may also change in the overburden. The direct impact of this on 4D seismic has not been thoroughly addressed in the literature. Here, laboratory data with an overburden shale core are presented, showing stress path dependent changes in P-wave velocity and pore pressure. The expected impact on 4D seismic can be significant.

Introduction

When a reservoir is depleted during hydrocarbon production or inflated during CO_2 storage, the change in pore pressure leads to stress changes in the surrounding rocks (Geertsma, 1973). The cap rock most often consists of shales with very low permeability. This means that fluid flow does not take place in short term, and that the response of the overburden can be assumed undrained.

Time-lapse (4D) seismic time shifts associated with overburden stress changes have been demonstrated to provide fingerprints of depletion in underlying reservoirs (Kenter *et al*., 2004; Hatchell and Bourne, 2005; Barkved and Kristiansen, 2004; Røste *et al*., 2006). The main effect is a slow-down of seismic waves in the overburden, associated with vertical stress decrease ($\leftrightarrow$ extension) in the overburden due to the effective stress increase ($\leftrightarrow$ compaction) in the reservoir. The impact of pore pressure changes on the 4D response was pointed out by Bauer *et al*. (2008), but appears to be neglected in conventional 4D data analysis.

The theoretical fundament for undrained pore pressure response in transversely isotropic media will be explained. Laboratory data are shown, comparing measured pore pressure changes with the theory. In addition, ultrasonic velocities were measured along different stress paths, and the impact of the pore pressure response on stress and stress path dependence will be addressed. Based on the laboratory data, the sensitivity of 4D travel time change to pore pressure change during depletion will be discussed.

Undrained pore pressure response

Skempton (1953) suggested the following equation for undrained pore pressure change (Δp_f), based on triaxial tests with clays:

$$\Delta p_f = B_S[\Delta\sigma_3 + A_S(\Delta\sigma_1 - \Delta\sigma_3)] \tag{1}$$

Here $\Delta\sigma_1$ and $\Delta\sigma_3$ are changes in maximum and minimum principal stress, respectively, while A_S and B_S are material parameters known as Skempton parameters. In linear isotropic poroelasticity, there is only one free Skempton parameter, B_S. The value of A_S should then be $= 1/3$, in order to ensure no pore pressure change in the case of constant mean stress. In experiments like those referred in Skempton's original paper, A_S can be very different from the elastic value. In shale, which is anisotropic, the Skempton-parameters should be considered part of a second order tensor. For transverse isotropy, which is a reasonable assumption for most unfractured shales, there are two independent and invariant Skempton parameters, B_V and B_H (e.g. Cheng, 1997). The subscripts V and H refer to vertical and horizontal; vertical is along the symmetry axis, whereas H is within the symmetry plane. The original Skempton parameters relate to the invariant material coefficients as

$$B_S = \frac{B_V + 2B_H}{3} \tag{2}$$

$$A_S(\theta) = \frac{B_V\cos^2\theta + B_H\sin^2\theta}{3B_S}$$

where θ is the angle between the symmetry axis and the maximum principal stress σ_1.

Link to rock physics

Assuming that wave velocities in shale under *in situ* conditions change linearly with changes in stress and pore pressure, the change in P- or S-wave velocities along any direction may be written (Holt *et al*., 2016):

$$\frac{\Delta v}{v} = A\Delta\bar{\sigma} + B\Delta(\sigma_1 - \sigma_3) - C\Delta p_f \tag{3}$$

$\Delta\bar{\sigma}$ is the change in mean stress, and the pore pressure change is denoted by Δp_f. A, B and C are coefficients expressing the stress sensitivity of the material. For isotropic incremental stress, the ratio C/A plays the role of an effective stress coefficient. Holt *et al*. (2016) demonstrated that laboratory measured P- and S-wave velocities follow a linear trend in in the stress path coefficient $\kappa = \Delta\sigma_3/\Delta\sigma_1$:

$$S = \frac{\Delta v}{v\Delta\sigma_1} = \frac{1+2\kappa}{3}A + (1-\kappa)B - C\frac{\Delta p_f}{\Delta\sigma_1} \tag{4}$$

This permits estimation of the three stress sensitivity parameters from experiments where various paths of stress and pore pressure change are probed.

Overburden pore pressure changes and 4D

In order to translate laboratory data to the field situation, one needs to replace the parameter κ with the *in situ* stress path. For the overburden, two stress path coefficients are defined:

$$\gamma_v = \frac{\Delta\sigma_v}{\Delta p_{f(res)}} \qquad (5)$$

$$\gamma_h = \frac{\Delta\sigma_h}{\Delta p_{f(res)}}$$

$\Delta p_{f(res)}$ refers to the pore pressure change in the reservoir. σ_v and σ_h are the vertical and horizontal stresses, respectively, while γ_v and γ_h are the vertical and horizontal stress path coefficients. Thus, provided the vertical is the maximum principal stress $\kappa = \gamma_h/\gamma_v$. The *in situ* sensitivity of wave velocities to reservoir pore pressure can then be written:

$$P = \frac{\Delta v}{v \Delta p_{f,res}} = \gamma_v S = \gamma_v \left\{ [\frac{A}{3} + B - A_S B_S C] + [\frac{2A}{3} - B - B_S(1 - A_S)C] \frac{\gamma_h}{\gamma_v} \right\} \quad (6)$$

Thus, there are three groups of parameters that influence the velocity changes, in addition to the driving force, i.e. the pore pressure change in the reservoir. These are:

- The *in situ* stress path, characterized by γ_v and γ_h. These parameters may be quantified by geomechanical modeling/simulations, and to some extent verified from in situ measurements, like time-lapse extended leak-off tests (XLOT). They reflect the geometry (aspect ratio and tilt) of the reservoir zone, the elastic contrast between the reservoir zone and the surroundings, and impact of non-elastic processes (Holt *et al*., 2016). The classical analytical solution assumes no elastic contrast (Geertsma, 1973) and predicts $\gamma_h/\gamma_v = -\frac{1}{2}$ (i.e. constant mean stress) throughout the overburden.
- The stress sensitivity of the rock itself, given by A, B and C (cfr. Eq(3)); which may be derived from laboratory experiments. Ultrasonic data were used in the current work, but there is evidence that stress sensitivities may be different at seismic frequencies (Holt *et al*., 2016).
- The Skempton parameters A_S and B_S (notice the angular dependence of A_S in Eq.(2)), quantifying the pore pressure change in the overburden as a result of undrained stress changes. As shown above, the Skempton parameters can be measured in core tests.

Laboratory experiments with a field shale

A preserved field shale core with 36 % porosity containing 65 weight % clay minerals has been drilled to cylindrical core plugs with 38 mm diameter and 50-60 mm length. The core plugs were brought to *in situ* stress and pore pressure, and are supposed to be fully saturated with native brine under such conditions. The samples were then probed along four different stress paths in a triaxial cell: Constant mean stress (CMS), $\kappa = -\frac{1}{2}$; triaxial (3AX), $\kappa = 0$; uniaxial strain (K_0), $\kappa = K_0$; and isostatic (ISO), $\kappa = 1$. All sequences were done as undrained loading–unloading cycles with 5 MPa axial stress change imposed in all cycles. In the laboratory tests, the axial stress is the maximum (corresponding to the *in situ* vertical stress), and denoted by σ_z. The confining stress is denoted by σ_r. The pore pressure response was measured in a 3 ml dead volume, ensuring good accuracy and acceptable time for pore pressure equilibration. In addition, axial and radial strains were recorded. Multidirectional ultrasonic (0.1 - 0.5 MHz) P- and S-wave velocities were obtained from pulse transmission measurements at each stress level after the pore pressure was equilibrated.

Figure 1 shows the pore pressure response normalized to the change in axial stress for each of the four stress paths in the shale for a plug drilled with the sample axis parallel to the symmetry axis (normal to bedding). The linear relationship with stress path is in perfect agreement with Skempton's law in Eq. (1) giving $A_S = 0.53$ and $B_S = 0.87$ (corresponding to $B_V = 1.38$ and $B_H = 0.61$).
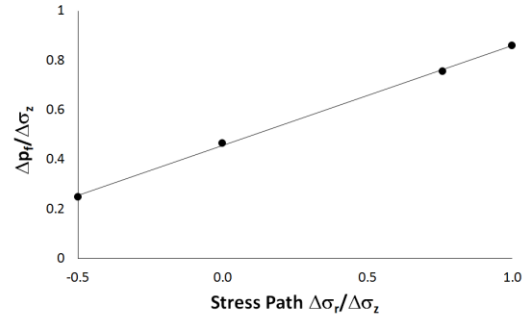

Figure 1: Change in pore pressure vs stress path parameter κ (= $\Delta\sigma_r/\Delta\sigma_z$) or laboratory tests with a field shale core having the sample (z-) axis normal to the bedding plane.

Two additional plugs with sample axis oriented within and at $45°$ to the bedding plane were tested along incrementally isostatic and triaxial stress paths. The angular dependence of A_S is shown in Figure 2. As can be seen, the trend is in accord with the theoretical angular dependence given in Eq. (2). The curve is drawn based on the values for B_V and B_H found from the test with the sample axis parallel to the symmetry axis shown in Figure 1. Considering that these measurements were performed with three different plugs, and that the orientation of the plugs was based on visual inspection, the results are considered in satisfactory agreement with theory. This implies that the deviation of the measured values from the isotropic value (=1/3) for Skempton's A_S parameter can be explained by anisotropy. For larger stress changes, non-elastic behavior will have a prominent influence on its value.
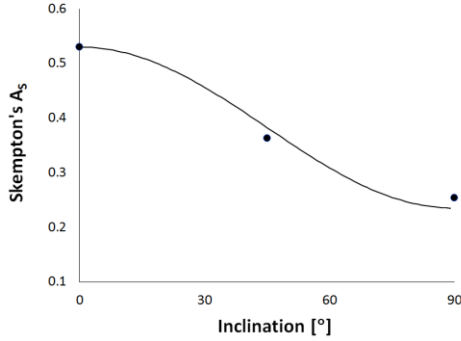
Overburden pore pressure changes and 4D

Figure 2 Change in pore pressure vs. inclination (angle between the axis of the sample and the symmetry axis) for laboratory tests with three differently oriented field shale core plugs. The curve is drawn according to Eq. (2)on the basis of measured A_S and B_S from the data shown in Figure 1.

The stress path dependent stress sensitivity of the ultrasonic P-wave velocity along the symmetry axis (v_{Pz}) is shown in Figure 3. Together with incrementally isostatic loading in drained and constant net stress conditions, this enables determination of the stress sensitivity coefficients (cf. Eq.(3)). They are: $A = 3.1$, $B = 0.8$, and $C = 2.3$; all in units of 10^{-2} MPa^{-1}. Thus, the effective stress coefficient under isostatic loading is 0.75 (=C/A). Even though small stress and pore pressure changes were enforced near the *in situ* stress, there are minor differences between coefficients representing unloading and loading. These differences will be neglected in this paper.

Also shown in Figure 3 is the strain sensitivity of the axial P-wave, denoted by R_{Pz}:

$$R_{Pz} = \frac{\Delta v_{Pz}}{v_{Pz}\Delta\varepsilon_z} \qquad (7)$$

$\Delta\varepsilon_z$ denotes the axial strain associated with an axial stress change $\Delta\sigma_z$. The strain is strongly dependent of stress path, which contributes to the stress path sensitivity of the R-factor, which, when accounting for anisotropy, can be written:

$$R_{Pz} = \left(\frac{\Delta v_{Pz}}{v_{Pz}\Delta\sigma_z}\right)\left(\frac{\Delta\sigma_z}{\Delta\varepsilon_z}\right) = S_{Pz}\frac{E_V}{1-(v_{VH}+v_{HV})\frac{E_V}{E_H}\kappa} \qquad (8)$$

The curve through the measured R-values in Figure 3 is obtained by fitting the anisotropic Young's moduli (E_V and E_H) and Poisson's ratios (v_{VH} and v_{HV}) to reproduce the measured trend.

Note that the stress path sensitivities both in S_{Pz} and R_{Pz} are very similar to those shown for a different field shale in Holt *et al.* (2016).
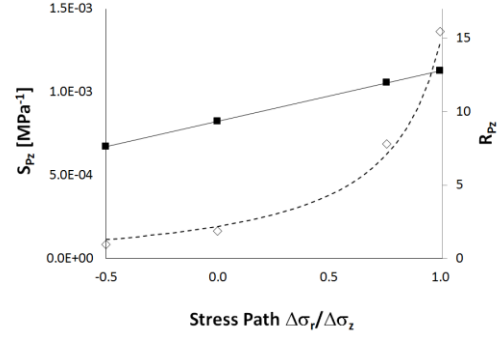

Figure 3   Laboratory measured ultrasonic stress and strain sensitivities S_{Pz} and R_{Pz} for axial P-wave velocity vs stress path parameter κ with a field shale core having the sample (z-) axis normal to the bedding plane (cf. Figure 1).

Discussion

The values of the Skempton-parameters depend on the drained, solid grain and pore fluid stiffnesses, in addition to anisotropy and plasticity. B_S will be close to 1 for a soft shale or a clay where the drained bulk modulus is negligible compared to that of the pore fluid, and close to 0 if the pore fluid is gas. In the latter case, because of the high gas compressibility, the pore pressure change is negligible, and the response is equivalent to that of a drained scenario.

In order to perform a sensitivity analysis, we assume that the overburden above a monitored reservoir consists of the same shale that has been studied experimentally, with the same properties. The stress arching coefficient γ_v is somewhat arbitrarily set to 0.1. We analyze only changes in the vertical P-wave velocity (Δv_{PV}), assuming undrained response and fully saturated overburden. Figure 4 shows that the stress sensitivity for all stress paths increases with decreasing B_S. The same trend is seen for the R-factor in Figure 5. The reduced P- and R – values compared to the laboratory results (Figure 5) is caused by the multiplication factor γ_v in Eq.(6).

The stress and stress path sensitivity of the P-wave velocity in a drained shale is clearly much higher than that for the undrained shale, since the drained stiffness (in particular the bulk modulus, controlling the behavior during isostatic loading; κ=1) is always smaller than the undrained stiffness. Thus, significant porosity change will contribute to P and R in the drained case, whereas the porosity change is negligible for the undrained scenario. With time, the initial undrained situation in the overburden will gradually transfer to a drained situation, leading to time-delayed velocity changes in the overburden. In a nanoDarcy shale, this time scale may be longer than field lifetime.
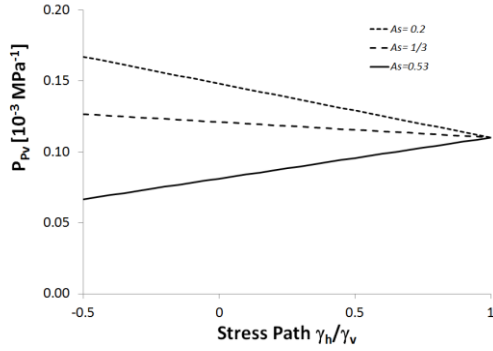
Figure 4 *In situ* sensitivity of vertical P-wave velocity to reservoir pore pressure change (P_{PV}, cfr Eq. (6)) vs *in situ* stress path for 3 different values of Skempton's B_S ($A_S = 0.53$). Ultrasonic stress sensitivity parameters are used (see text); $\gamma_v = 0.1$.
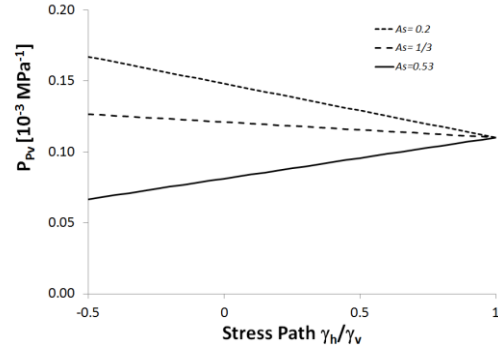

Figure 6 *In situ* sensitivity of vertical P-wave velocity to reservoir pore pressure change (P_{PV}, cfr Eq. (6)) vs *in situ* stress path for 3 different values of Skempton's A_S ($B_S = 0.87$). Ultrasonic stress sensitivity parameters are used (see text).; $\gamma_v = 0.1$.
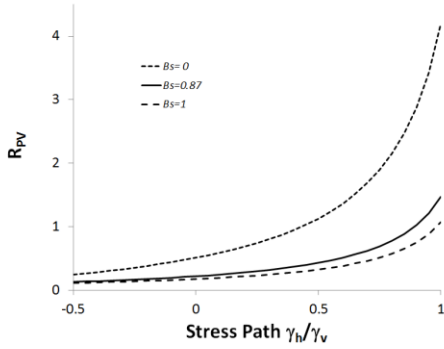

Figure 5 Vertical P-wave velocity strain sensitivity (R_{PV}) vs *in situ* stress path for 3 different values of Skempton's B_S ($A_S = 0.53$). Ultrasonic stress sensitivity parameters are used (see text).
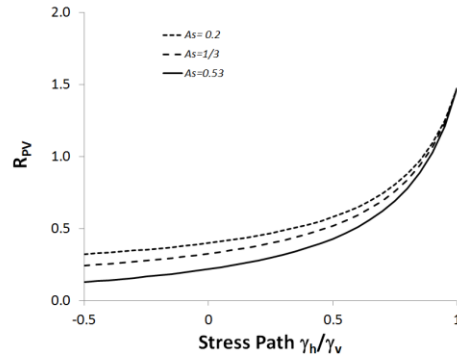

Figure 7 Vertical P-wave velocity strain sensitivity (R_{PV}) vs *in situ* stress path for 3 different values of Skempton's A_S ($B_S = 0.87$). Ultrasonic stress sensitivity parameters are used (see text).

The influences of A_S on *in situ* stress and strain sensitivity are illustrated in Figure 6 and Figure 7. As expected A_S has no influence for an isostatic stress path, but decreasing A_S leads to strongly increased stress sensitivity for lower values of the stress path expressed by γ_h/γ_v. Notice that the value of A_S may vary widely. From our work, it is clearly linked to the degree of anisotropy, and to the orientation of principal stress with respect to bedding. From triaxial data near failure, values close to 1 were obtained for A_S for normally consolidated clays, whereas negative values were obtained for overconsolidated clays (Bishop and Henkel, 1962).

Conclusion

Laboratory experiments with a high porosity clay rich shale shows that pore pressure evolution under different stress paths are controlled by Skempton parameters as expected

on basis of transverse isotropy. Combining pore pressure and ultrasonic velocity measurements, stress path dependent stress and strain dependences can be determined. Using these as input data for addressing the same parameters under *in situ* conditions shows that the *in situ* stress path and the associated pore pressure evolution (and hence the values of the Skempton parameters) have fundamental and significant impact on two-way travel times in 4D seismic.

Acknowledgements

Overburden pore pressure changes and 4D

REFERENCES:

Barkved, O. and T.G. Kristensen, 2005, Seismic time-lapse effects and stress changes: Examples from a compacting reservoir: The Leading Edge 24 (12) 1244 – 1248, doi: 10.1190/1.2149636.

Bauer, A., C. Lehr, F. Korndorffer, A. van der Linden, J. Dudley, T. Addis, K. Love, and M. Myers, 2008. Stress and pore-pressure dependence of sound velocities in shales: Poroelastic effects in timelapse seismic. SEG Abstract; 4 pp.

Bishop, A.W. and D.J. Henkel, 1962. *The measurement of soil properties in the triaxial test*. Arnold,London. 190 pp.
Cheng, A. H.-D., 1997. Material coefficients of anisotropic poroelasticity. Int. J. Rock mech. & Min. Sci. 34, 199-205.

Geertsma, J., 1973, A basic theory of subsidence due to reservoir compaction: The homogeneous case: Verhandelingen Kon. Ned. Geol. Mijnbouwk. Gen. 28, 43-62.

Hatchell, P. and S. Bourne, 2005, Rocks under strain: Strain-induced time-shifts are observed for depleting reservoirs: The Leading Edge, 24, 1222-1225, doi: 10.1190/1.2149624.

Holt, R.M., A. Bauer, A. Bakk, and D. Szewczyk, 2016. Stress path dependence of ultrasonic and seismic velocities in shale. SEG Abstract, 4 pp.

Kenter C.J., A.C. van den Beukel, P.J. Hatchell, K P. Maron, M.M. Molenaar, and J. G.F. Stammeijer, 2004, Geomechanics and 4D: Evaluation of reservoir characteristics from timeshifts in the overburden: Proceedings of Gulf Rocks'04, ARMA-04-627, 8 pp.

Røste, T., A. Stovas, and M. Landrø, 2006, Estimation of layer thickness and velocity changes using 4D prestack seismic data: Geophysics, **71** (6), S219–S234, doi: 10.1190/1.2335657.

Skempton, A.W., 1954, The pore pressure coefficients *A* and *B*: Géotechnique **4**, 143-147, doi: 10.1680/geot.1954.4.4.143.